

CLASH: DISCOVERY OF A BRIGHT $z \simeq 6.2$ DWARF GALAXY QUADRUPLY LENSED BY MACS J0329.6-0211

A. ZITRIN¹, J. MOUSTAKAS², L. BRADLEY³, D. COE³, L.A. MOUSTAKAS⁴, M. POSTMAN³, X. SHU⁵, W. ZHENG⁶, N. BENÍTEZ⁷, R. BOUWENS⁸, T. BROADHURST^{9,10}, H. FORD⁶, O. HOST¹¹, S. JOUVEL¹¹, A. KOEKEMOER³, M. MENEGHETTI¹², P. ROSATI¹³, M. DONAHUE¹⁴, C. GRILLO¹⁵, D. KELSON¹⁶, D. LEMZE⁶, E. MEDEZINSKI⁶, A. MOLINO⁷, M. NONINO¹⁷, AND S. OGAZ³

Submitted to the Astrophysical Journal Letters

ABSTRACT

We report the discovery of a $z_{\text{phot}} = 6.18^{+0.05}_{-0.07}$ (95% confidence level) dwarf galaxy, lensed into four images by the galaxy cluster MACS J0329.6-0211 ($z_l = 0.45$). The galaxy is observed as a high-redshift dropout in *HST*/ACS/WFC3 CLASH and *Spitzer*/IRAC imaging. Its redshift is securely determined due to a clear detection of the Lyman-break in the 18-band photometry, making this galaxy one of the highest-redshift multiply-lensed objects known to date with an observed magnitude of $F125W = 24.00 \pm 0.04$ AB mag for its most magnified image. We also present the first strong-lensing analysis of this cluster uncovering 15 additional multiply-imaged candidates of five lower-redshift sources spanning the range $z_s \simeq 2 - 4$. The mass model independently supports the high photometric redshift and reveals magnifications of $11.6^{+8.9}_{-4.1}$, $17.6^{+6.2}_{-3.9}$, $3.9^{+3.0}_{-1.7}$, and $3.7^{+1.3}_{-0.2}$, respectively, for the four images of the high-redshift galaxy. By delensing the most magnified image we construct an image of the source with a physical resolution of ~ 200 pc when the universe was ~ 0.9 Gyr old, where the $z \simeq 6.2$ galaxy occupies a source-plane area of approximately 2.2 kpc^2 . Modeling the observed spectral energy distribution (SED) using population synthesis models, we find a demagnified stellar mass of $\sim 10^9 M_\odot$, subsolar metallicity ($Z/Z_\odot \sim 0.5$), low dust content ($A_V \sim 0.1$ mag), a demagnified SFR of $\sim 3.2 M_\odot \text{ yr}^{-1}$, and a specific SFR of $\sim 3.4 \text{ Gyr}^{-1}$, all consistent with the properties of local dwarf galaxies.

Subject headings: dark matter, galaxies: clusters: individuals: MACS J0329.6-0211, galaxies: clusters: general, galaxies: high-redshift, gravitational lensing: strong

1. INTRODUCTION

By gravitationally lensing distant background sources, galaxy clusters act as natural magnifying lenses in the sky, providing a unique window into the early Universe. Several high-redshift galaxies have been discovered through the magnification power of galaxy clusters (e.g. Franx et al. 1997; Frye et al. 2002; Bouwens et al. 2009b; Zheng et al. 2009; Bradley et al. 2011). The current

highest-redshift lensed galaxy is at $z = 7.6$ in the field of Abell 1689 (Bradley et al. 2008), but among the highest-redshift *multiply-lensed* galaxies known are a galaxy at $z = 6.03$ in the field of Abell 383 (comprising two images; Richard et al. 2011; Zitrin et al. 2011c), a $z \sim 6.5$ galaxy in the field of Abell 2218 (comprising three images; Kneib et al. 2004; Egami et al. 2005), and a $z \sim 7$ candidate in the “bullet cluster” (comprising two images; Hall et al. 2011). In addition, the lens model can be used to map the lensed images back into the source plane, while the high magnification enables their spatially resolved internal structural properties to be measured. Such measurements are not possible without the aid of the lensing power of the cluster (e.g. Zitrin et al. 2011b).

The Lyman-alpha forest produces a sharp drop in flux below 1216 \AA . The expansion of the universe moves this spectral break to longer wavelengths, allowing high-redshift galaxies to be identified as “dropouts” in the observed-frame optical and near-IR (see Madau 1995; Franx et al. 1997). As these young, high-redshift galaxies are usually actively forming stars, their rest-frame UV spectra should be relatively blue. This combination of properties allows the redshift of the galaxy to be estimated accurately, even without spectroscopy: as low as $\sim 1\%$ uncertainty on the redshift is obtained here, for 95% confidence levels. The study of high-redshift galaxies enables important constraints to be placed on galaxy evolution and structure formation. Particularly, observing high-redshift galaxies provides direct measurements of the high- z luminosity-function, early SFR, and the epoch of the intergalactic medium reionization (see

¹ Institut für Theoretische Astrophysik, Universität Heidelberg; adizitrin@gmail.com

² Center for Astrophysics and Space Sciences, University of California, San Diego

³ Space Telescope Science Institute, Baltimore

⁴ Jet Propulsion Laboratory, California Institute of Technology

⁵ University of Science and Technology of China, Hefei, Anhui

⁶ Department of Physics and Astronomy, The Johns Hopkins University

⁷ Instituto de Astrofísica de Andalucía (CSIC)

⁸ Leiden Observatory, University of Leiden

⁹ Department of Theoretical Physics, University of Basque Country

¹⁰ IKERBASQUE, Basque Foundation for Science

¹¹ Department of Physics & Astronomy, University College London

¹² INAF, Osservatorio Astronomico di Bologna; INFN, Sezione di Bologna

¹³ European Southern Observatory

¹⁴ Physics and Astronomy Department, Michigan State University

¹⁵ Excellence Cluster Universe, Technische Universität München

¹⁶ Observatories of the Carnegie Institution of Washington, Pasadena

¹⁷ INAF-Osservatorio Astronomico di Trieste

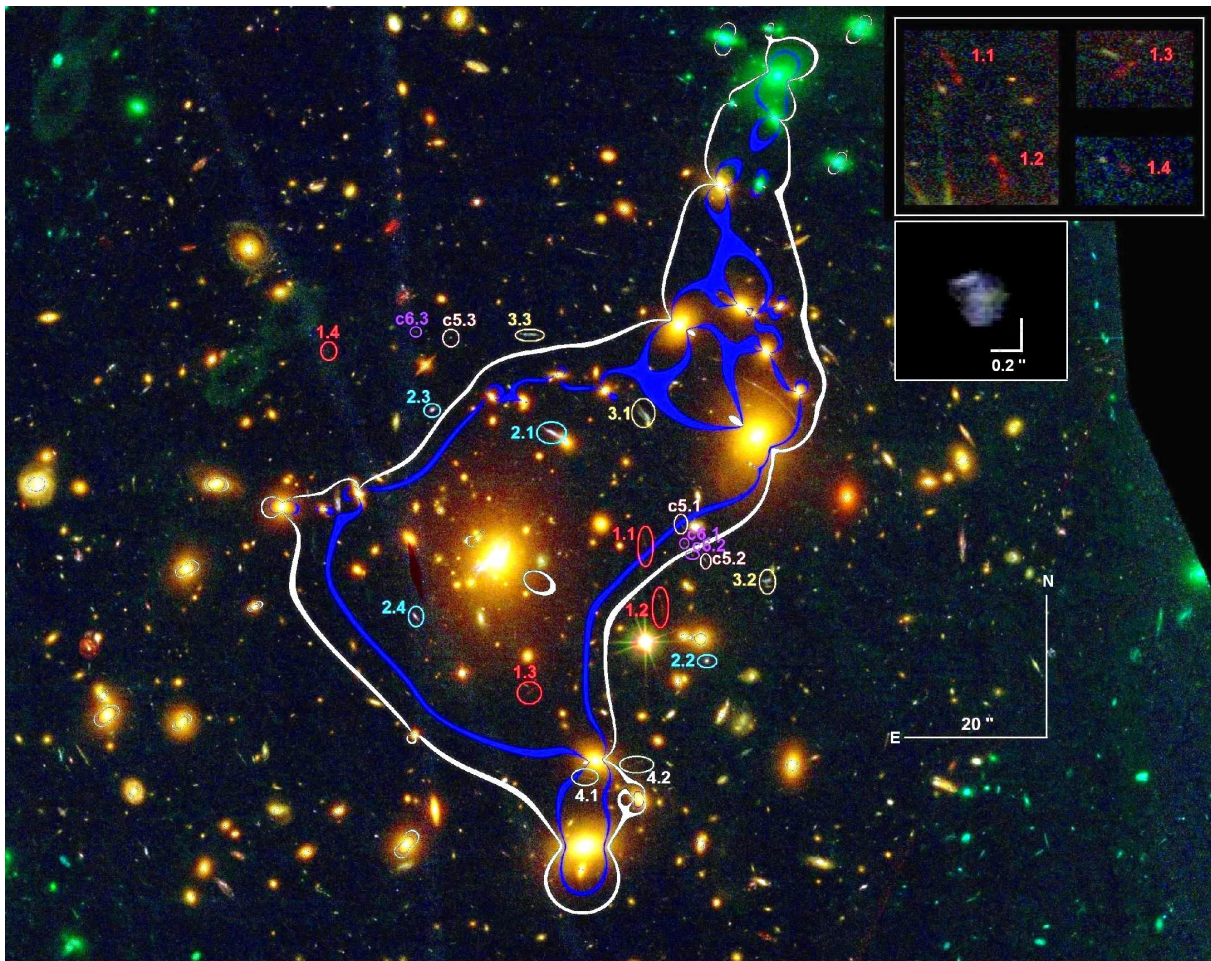


FIG. 1.— Galaxy cluster MACS0329 ($z = 0.45$) imaged with *HST*/ACS/WFC3. We number the multiple-images uncovered by our model, where the two candidate systems are marked in “c”. All systems are accurately reproduced by our model, with an average image-plane reproduction uncertainty of $2.07''$ per image, and image-plane *rms* of $2.32''$, excluding candidate systems. The white critical curve corresponds to system 1 at $z_s = 6.18$, and the blue critical curve corresponds to system 2 at $z_s = 2.17$. The composition of this color image is Red=F105W+F110W+F125W+F140W+F160W, Green=F606W+F625W+F775W+F814W+F850LP, and Blue=F435W+F475W. The *upper-right* inset shows a blow-up of the $z = 6.18$ system, below which we inset the source-galaxy as reproduced by our model by delensing the most magnified image 1.2 ($\mu \sim 17.6$) to the source plane, yielding a resolution of ~ 200 pc per pixel. Overplotted therein are bars showing the source-plane size of $0.2''$ ($\simeq 1.2$ kpc). Noise cleaning and color manipulation procedures were performed for a better view of the internal details of the source.

Bradley et al. 2011, and references therein).

We report the discovery of one of the highest-redshift ($z_{\text{phot}} = 6.18^{+0.05}_{-0.07}$) multiply-lensed galaxies known to date, lensed into four images by the galaxy cluster MACS J0329.6-0211 ($z=0.45$; MACS0329 hereafter). MACS0329 is an X-ray selected system found by the Massive Cluster Survey, MACS (Ebeling et al. 2001, 2010). Maughan et al. (2008) classified MACSJ0329 as having evidence for substructure in its X-ray surface brightness, although Schmidt & Allen (2007) classified it as relaxed. We found no record of previous strong lensing (SL) analysis of this cluster, and only 1-band shallow *HST*/WFPC2 previous imaging. The 16 *HST* bands chosen for the Cluster Lensing and Supernova survey with Hubble (CLASH; Postman et al. 2011) enable us to conduct the first SL study of this cluster, and to obtain accurate photometric redshifts for the multiply-lensed background galaxies. We use these data in conjunction with a parametric SL modeling method (e.g., Broadhurst et al. 2005; Zitrin et al. 2009, 2011a,b; Merten et al. 2011), to find several multiple image families across

the central field of MACS0329 (Fig. 1) so that its mass distribution and inner profile can be well-constrained, allowing us to deduce the source-plane properties of the high-redshift galaxy presented here.

The paper is organized as follows: In §2 we describe the observations, and in §3 we detail the SL model. In §4 we report the results of the SL analysis and the physical properties of the high-redshift galaxy based on detailed SED modeling. The results and conclusions are summarized in §5. We adopt a concordance Λ CDM cosmology with $\Omega_{m0} = 0.3$, $\Omega_{\Lambda0} = 0.7$, and $h = 0.7$. With these parameters, one arcsecond corresponds to a physical scale of 5.76 kpc at the cluster redshift ($z = 0.45$; Allen et al. 2008), and 5.62 kpc at $z = 6.18$.

2. OBSERVATIONS AND REDSHIFTS

MACS0329 was observed as part of CLASH with *HST* from 2011 August to 2011 October. This is one of 25 clusters to be observed to a total depth of 20 *HST* orbits in 16 filters with the Wide Field Camera 3 (WFC3) UVIS and IR cameras, and the Advanced Camera for Surveys (ACS) WFC. The images are reduced and mo-

saiced ($0''.065 \text{ pixel}^{-1}$) using standard techniques implemented in the *MosaicDrizzle* pipeline (Koekemoer et al. 2002, 2011). HST photometry for the arcs is obtained within the apertures shown in Fig. 2, and photometric redshifts are estimated for all the galaxies in the field using the full 16-band UVIS/ACS/WFC3-IR aperture-matched (e.g., Fig 2) photometry via both the BPZ (Benítez 2000; Benítez et al. 2004; Coe et al. 2006) and LePhare (Arnouts et al. 1999; Ilbert et al. 2006) programs. See Postman et al. (2011) for additional details.

We supplement these *HST* observations with Infrared Array Camera (IRAC) imaging obtained in 2011 October as part of the *Spitzer* Cycle 8 warm mission (PI: R. Bouwens; see also Postman et al. 2011). The Warm *Spitzer* IRAC observations in Channels 1 and 2 (3.6 and $4.5 \mu\text{m}$) have a total integration time of $13,290\text{s}$, and clearly detect three of the four images of the background source we report here (1.1 through 1.3), with a formal $\sim 2\sigma$ detection for arc 1.4. Because of crowding in the *Spitzer* images, we adopt a circular $2.4''$ diameter aperture for the IRAC photometry. Background levels are estimated by sampling non-crowded sections of the IRAC mosaic while avoiding nearby bright sources. The accuracy of this (manual) photometry is verified by subtracting possible contaminating sources with GALFIT¹, especially for arc 1.2 which has a bright star nearby. We use a flux aperture correction factor of $1.9\times$, based on a curve of growth analysis of unresolved sources in the Post Basic Calibrated Data (PBCD) mosaic. The relevant multi-wavelength photometry is given in Table 1.

3. STRONG LENSING MODELING AND ANALYSIS

The lens modeling method used here (e.g., Broadhurst et al. 2005; Zitrin et al. 2009) begins with the assumption that mass approximately traces light. We model the distribution of cluster mass by assigning a power-law mass profile to each red-sequence cluster galaxy, scaled by its (relative) brightness. The sum of all galaxy contributions represents the lumpy galaxy component, which is then smoothed using 2D spline interpolation to obtain a smooth-component representing the dark matter (DM) distribution. The polynomial degree of smoothing and the index of the power-law are the most important free parameters determining the mass profile.

A worthwhile improvement in fitting the location of the lensed images is generally found by introducing an external shear describing the overall matter ellipticity. The direction of the shear and its amplitude are free parameters, allowing for some flexibility in the relation between the distribution of DM and the distribution of galaxies. The weight of the lumpy component relative to the DM, and the overall normalization, bring the total number of free parameters in our modeling to six (see Zitrin et al. 2009).

The best fit is assessed by a χ^2 minimization in the image plane, which is preferred because it generally does not produce solutions that are biased towards shallow mass profiles (and high magnifications), as is the case with source-plane minimization. The positions and morphologies of the multiply-imaged arcs are accurately reproduced by the best-fit mass model in their measured photometric redshifts (for a morphological comparison

example see Fig. 4), and the model is successively refined as additional sets of multiple images are incorporated.

4. RESULTS

We uncovered in *HST*/CLASH and *Spitzer*/IRAC imaging of MACS0329 one of the highest-redshift multiply-lensed galaxies known to date. We use the independent photometric-redshift distributions of its four lensed images to obtain a source redshift (and 2σ limits, see Table 1) of $z_{\text{phot}} = 6.18^{+0.05}_{-0.07}$. Using our mass model and the extensive imaging and resulting photometric redshifts, we physically matched 15 additional new multiple images and candidates of five background, lower- z sources (see Figure 1), which are used in turn to refine the mass model. Explicitly, in addition to the four images of the high- z galaxy, we use as additional constraints the seven multiple-images of systems 2 and 3, at photometric redshifts (and 2σ limits) of $z_s = 2.17^{+0.12}_{-0.03}$ and $z_s = 2.89^{+0.05}_{-0.05}$, respectively, and verify that all other systems and candidates are plausible in the context of the resulting mass model.

The magnification by the cluster is coupled to the surface-density gradient in each point (i.e., the mass profile), so multiple-systems with redshift information are important to assess the true magnification across the cluster field. For the four images of the $z_{\text{phot}} = 6.18$ galaxy, we obtain magnifications (and 1σ uncertainties) of $11.6^{+8.9}_{-4.1}$, $17.6^{+6.2}_{-3.9}$, $3.9^{+3.0}_{-1.7}$, and $3.7^{+1.3}_{-0.2}$, respectively, so that in total the galaxy is magnified by a factor of $\simeq 37$.

We leverage the magnification boost of the most magnified image, arc 1.2, to construct a high-resolution image of the background galaxy, which occupies a source-plane area of $\sim 2.2 \text{ kpc}^2$ (see Figure 1). To further constrain the physical properties of this galaxy, we model the observed SED of arc 1.2 using the Bayesian SED-fitting code *iSEDfit* (see Moustakas et al. 2011) coupled to the flexible stellar population synthesis models of Conroy et al. (2009). We adopt the Chabrier (2003) initial mass function from $0.1 - 100 \mathcal{M}_{\odot}$, assume the Calzetti et al. (2000) dust attenuation law, and adopt uniform priors (based on Monte Carlo draws) on the stellar metallicity ($0.0002 < Z < 0.03$), V-band attenuation ($0 < A_V < 2 \text{ mag}$), and galaxy age ($0.005 - 1 \text{ Gyr}$). For reference, the age of the universe at $z = 6.18$ is 0.9 Gyr . We parameterize the star formation history $\psi(t)$ as an exponentially declining function of time, t , given by $\psi(t) \propto \exp(-t/\tau)$, where τ is the characteristic time for star formation. We draw τ from a uniform distribution between $0.01 - 5 \text{ Gyr}$, which spans the range from passively evolving to continuous star formation.

In Figure 3 we show the observed and rest-frame SED of arc 1.2, the maximum likelihood model fit, and the posterior distributions on all the model parameters. Adopting the median of each posterior distribution as our best estimate of the properties of the galaxy, we find a demagnified stellar mass of $\sim 10^9 \mathcal{M}_{\odot}$, low dust content ($A_V \sim 0.1 \text{ mag}$), a demagnified SFR of $\sim 3.2 \mathcal{M}_{\odot} \text{ yr}^{-1}$, and a SFR-weighted age of $\sim 180 \text{ Myr}$. These results imply a specific SFR, $\text{sSFR} \equiv \text{SFR}/\mathcal{M}$, of $\sim 3.4 \text{ Gyr}^{-1}$, corresponding to a mass-doubling time of just 600 Myr (assuming a 50% return fraction). The stellar metallicity and τ parameter (not shown) are not particularly well constrained, although solutions with subsolar metal-

¹ <http://users.obs.carnegiescience.edu/peng/work/galfit/galfit.html>

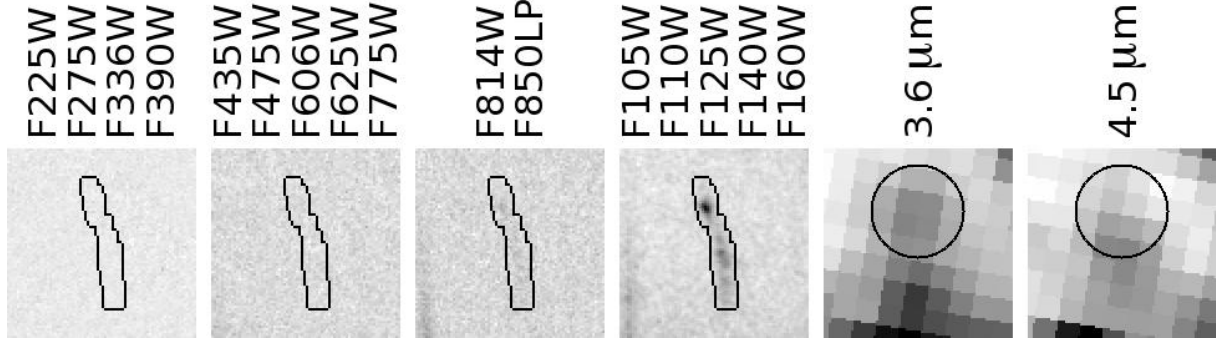


FIG. 2.— Thumbnails ($5'' \times 5''$) of the four arcs of the $z = 6.18$ source in the different bands, with tailored apertures used for the photometry overlaid. As is clear, these are not seen below the F814W band, in agreement with the photometric redshift estimate. See Fig. 3 and Table 1 for the SED and photometry, respectively.

TABLE 1
MULTIPLE-IMAGES DATA AND MULTIBAND PHOTOMETRY FOR THE FOUR IMAGES OF THE $z = 6.18$ GALAXY

ARC ID	RA (J2000.0)	DEC (J2000.0)	BPZ z_{phot} (best) [95% C.L.]			LPZ z_{phot} (best) [95% C.L.]			Magnification, μ	
1.1	03:29:40.18	-02:11:45.60	6.185 [6.079–6.282]			6.155 [5.885–6.374]			$11.6^{+8.9}_{-4.1}$	
1.2	03:29:40.06	-02:11:51.72	6.137 [6.024–6.204]			6.194 [5.982–6.347]			$17.6^{+6.2}_{-3.9}$	
1.3	03:29:41.28	-02:12:05.04	6.152 [6.055–6.257]			6.253 [5.828–6.573]			$3.9^{+3.0}_{-1.7}$	
1.4	03:29:43.16	-02:11:17.30	6.246 [6.073–6.395]			5.965 [5.482–6.327]			$3.7^{+1.3}_{-0.2}$	
Multi-band photometry										
ARC	F775W	F814W	F850LP	F105W	F110W	F125W	F140W	F160W	3.6 μm	4.5 μm
1.1	26.24 \pm 0.32	25.69 \pm 0.12	24.73 \pm 0.11	24.41 \pm 0.05	24.39 \pm 0.04	24.46 \pm 0.05	24.52 \pm 0.04	24.62 \pm 0.05	24.4 \pm 0.2	24.7 \pm 0.3
1.2	> 26.52 (2 σ)	25.32 \pm 0.10	24.29 \pm 0.08	23.94 \pm 0.04	23.90 \pm 0.03	24.00 \pm 0.04	24.04 \pm 0.03	24.11 \pm 0.04	23.6 \pm 0.2	23.5 \pm 0.1
1.3	26.52 \pm 0.33	26.30 \pm 0.17	25.52 \pm 0.17	24.83 \pm 0.06	24.93 \pm 0.05	24.87 \pm 0.06	24.91 \pm 0.05	25.01 \pm 0.06	24.9 \pm 0.6	24.5 \pm 0.3
1.4	> 29.94 (2 σ)	> 27.76 (2 σ)	25.28 \pm 0.14	26.17 \pm 0.13	26.25 \pm 0.10	26.54 \pm 0.17	26.42 \pm 0.13	26.28 \pm 0.13	24.8 \pm 0.2	> 24.9 (2 σ)

NOTE. — Data for the multiple images of the $z = 6.18$ galaxy. *Top*: Columns are: arc ID; RA and DEC; photo- z using BPZ and LePhare (hereafter LPZ), respectively; μ , magnification predicted by the mass model. *Bottom*: Multiband photometry for the dropout band (F775W) and all redder bandpasses, for the four images of the $z = 6.18$ galaxy, in AB mags. Lower (2σ) limits are given for non-detections; we find no 2σ detections in any of the 8 bluer bands. Note also that the (relative) magnitudes between the different images of this system agree overall with the (relative) magnifications derived by our mass model (see §4), with some deviation for the less magnified images, 1.3(1.4), which seem slightly less(more) magnified than our model implies.

licity and $\tau \gg 0$ Gyr are generally favored; the median of the posterior distributions imply subsolar metallicity, $Z/Z_{\odot} \sim 0.5$, and $\tau \sim 2.4$ Gyr.

We verified that performing our SED modeling on the other (less magnified) images yields overall similar results. The demagnified SED of arc 1.1 is nearly identical to that of arc 1.2, and therefore the posterior distributions of the physical quantities we derive are very similar to those shown in Figure 3; the median quantities all agree to well within 0.1 dex ($\pm 50\%$). The demagnified F125W magnitude of arc 1.3(1.4), on the other hand, is 0.8 mag brighter(fainter) than arcs 1.1 and 1.2, although this discrepancy is well within the statistical uncertainties on the magnifications. Nevertheless, at face value the fainter two arcs imply an 0.3-0.4 dex larger stellar mass and SFR, 0.2-0.6 mag more dust attenuation, and a very similar age, 200 Myr. However, we emphasize that the posterior distributions on these quantities overlap significantly with those of arcs 1.1 and 1.2, and therefore these differences do not affect our conclusions about the nature of this object.

Note also that the center of emission in the $3.6\mu m$ image is slightly different than that of the $4.5\mu m$ image (Figure 2). Repeating the photometry on the two dif-

ferent centers, we find this offset may introduce uncertainty of ~ 0.3 mag in the IRAC photometry. The effect of possible contamination from bright neighbors was re-examined for both emission-centers, and was found to be typically 0.4 mag. However, we importantly verified that these higher uncertainties have only a negligible (< 0.1 dex) effect on the resulting physical properties, as the fit is governed by the HST photometry.

Finally, we use our lens model to constrain the physical characteristics of MACS0329. For the $z_s = 6.18$ source, the critical curves enclose a relatively large area, with an effective Einstein radius of $r_E = 33''.9 \pm 3''$ ($\simeq 195$ kpc at $z_l = 0.45$), and a projected mass of $1.89^{+0.10}_{-0.06} \times 10^{14} M_{\odot}$ (Figure 1). For the lower redshift of system 2, $z_s = 2.17$, the Einstein radius is $\simeq 27''.7$, and the critical curve encloses a projected mass of $1.40^{+0.09}_{-0.05} \times 10^{14} M_{\odot}$. For completeness, we measure the (total) mass profile slope, $d \log \Sigma / d \log r \simeq -0.61^{+0.05}_{-0.1}$ (in the range $1'' - 52''$, or $6 \lesssim r \lesssim 300$ kpc; about twice the Einstein radius for $z_s \sim 2$), typical of *relaxed* and well-concentrated lensing clusters (e.g. Broadhurst et al. 2005; Zitrin et al. 2009), and in agreement with the fairly circularly-symmetric X-ray contours centered on the BCG (see Mann & Ebeling

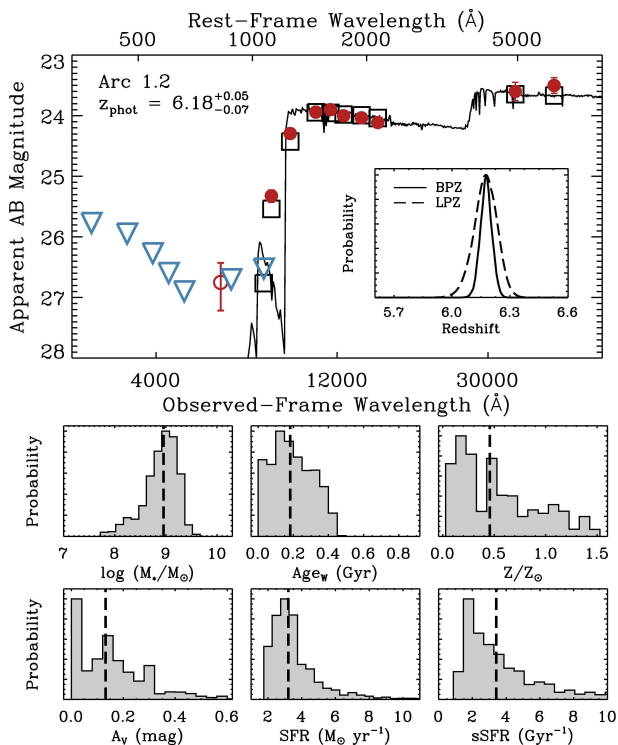


FIG. 3.— SED modeling results of arc 1.2, the most magnified image of the $z_{\text{phot}} \simeq 6.18$ galaxy. The upper panel shows the observed and rest-frame SED and the maximum likelihood model fit. The filled red points indicate bands in which the object is well detected, while the open blue triangles indicate 2σ upper limits; the open squares show the photometry of the best-fitting model convolved with the WFC3, ACS, and IRAC filter response functions. The open red circle indicates a spurious, marginally significant detection of arc 1.2 in the F606W band; however, we emphasize that none of the other images are detected in this band. We also show an inset with the photometric redshift distribution, $P(z)$, obtained by combining the independent photometric redshift measurements of the four arcs, yielding a source redshift of $z = 6.18^{+0.05}_{-0.07}$ with BPZ, and $6.18^{+0.11}_{-0.13}$ with LPZ (95% confidence levels). The lower panels show the posterior distributions on the demagnified stellar mass, SFR weighted age, stellar metallicity (relative to $Z_{\odot} = 0.019$), rest V-band dust attenuation, demagnified SFR, and specific SFR, $\text{sSFR} \equiv \text{SFR}/M$. The vertical dashed lines show the median of each posterior distribution. We summarize the results in §4.

2011).

5. DISCUSSION AND CONCLUSIONS

The discovery of a high-redshift galaxy in the field of MACS0329 adds to several known high-redshift galaxies lensed by galaxy clusters (e.g., Egami et al. 2005; Bradley et al. 2008, 2011; Zheng et al. 2009; Richard et al. 2011). Here we summarize the properties of this unique source.

(1) It is one of the highest-redshift multiply lensed objects known to date, and lensed into four separate images. The angular separation between arcs 1.2 and 1.4 is $\sim 1'$, considerably larger than previously reported cases (Egami et al. 2005; Richard et al. 2011).

(2) The source is one of the brightest at $z > 6$: its J_{125} magnitude is 24.0 AB, making it a viable candidate for follow-up spectroscopy.

(3) The galaxy is consistent with being a dwarf galaxy. Its intrinsic (delensed) magnitude of $J_{125} = 27.1$ AB makes it a sub- L_* galaxy at this redshift. It occupies

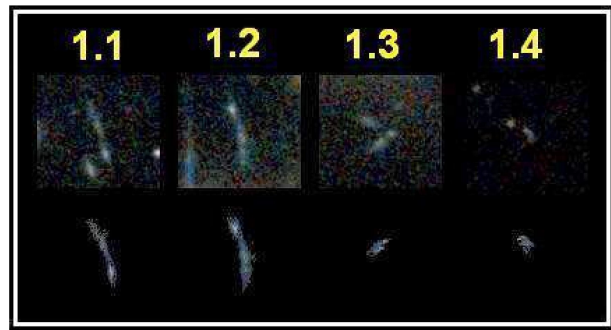


FIG. 4.— Reproduction of systems 1 by our model (lower row), compared with the real images (upper row). We delens image 1.1 to the source plane and relens it back to the image-plane to reproduce the other images of this system. As can be seen, our model reproduces well the images of this system. Note also, our model requires larger deflection angles for the $z = 6.18$ source, relative to lower- z systems such as systems 2 and 3, independently strengthening its detection as a high-redshift source.

a source-plane area of $\sim 2.2 \text{ kpc}^2$, similar to previously deduced sizes of high- z lensed galaxies (e.g. Zitrin et al. 2011b). Due to the hierarchical growth of structure, galaxies are expected to be small at high redshifts, with dwarf galaxies constituting the building material of larger structures. Our source-plane reconstruction shows at least three (possibly star-forming) knots, consistent with several other reports of high-redshift galaxies with multiple components (Franx et al. 1997; Bradley et al. 2008, 2011; Zheng et al. 2009; Oesch et al. 2010; Zitrin et al. 2011b), possibly as the result of merging. In addition, we measure an overall half-light radius of $\sim 0.12''$, consistent with that found in Bouwens et al. (2004, 2006) and (Oesch et al. 2010).

(4) The SED fits to the multiband photometry of the source suggest a demagnified stellar mass of $\sim 10^9 M_{\odot}$, a SFR-weighted age of $\sim 180 \text{ Myr}$, subsolar metallicity ($Z/Z_{\odot} \sim 0.5$), low dust content ($A_V \sim 0.1 \text{ mag}$), and a demagnified SFR of $\sim 3.2 M_{\odot} \text{ yr}^{-1}$. The specific SFR of $\sim 3.4 \text{ Gyr}^{-1}$, which is slightly higher than that found by other recent studies (Gonzalez et al. 2011; Stark et al. 2009; Labbé et al. 2010; McLure et al. 2011), implies a mass-doubling time of just 600 Myr and therefore vigorous ongoing star formation considering its low mass.

(5) The UV continuum is blue, with a UV-slope $\beta = -2.5 \pm 0.06$, consistent with measurements of other faint $z \sim 6$ galaxies and suggests that these sources are largely dust free (Bouwens et al. 2009a, 2011; Finkelstein et al. 2011; Vanzella et al. 2011).

The discovery of the galaxy presented here shows once more the novelty and tremendous potential of galaxy clusters for observationally accessing the faint early universe.

ACKNOWLEDGMENTS

The authors thank Saurabh Jha for useful discussions, and the anonymous referee for valuable comments. The CLASH Multi-Cycle Treasury Program (GO-12065) is based on observations made with the NASA/ESA Hubble Space Telescope. The Space Telescope Science Institute is operated by the Association of Universities for Research in Astronomy, Inc. under NASA contract NAS 5-26555. This work is based in part on observations

made with the *Spitzer* Space Telescope, which is operated by the Jet Propulsion Laboratory, California Institute of Technology under a contract with NASA. Support for this work was provided by NASA through an

award issued by JPL/Caltech. We thank the hospitality of Institut für Theoretische Astrophysik, Universität Heidelberg, where part of this work took place, and the Baden-Württemberg Stiftung.

REFERENCES

- Allen, S. W., Rapetti, D. A., Schmidt, R. W., Ebeling, H., Morris, R. G., & Fabian, A. C. 2008, *MNRAS*, 383, 879
- Arnouts, S., Cristiani, S., Moscardini, L., Matarrese, S., Lucchin, F., Fontana, A., & Giallongo, E. 1999, *MNRAS*, 310, 540
- Benítez, N. 2000, *ApJ*, 536, 571
- Benítez, N., et al. 2004, *ApJS*, 150, 1
- Bouwens, R. J., Illingworth, G. D., Blakeslee, J. P., Broadhurst, T. J., & Franx, M. 2004, *ApJ*, 611, L1
- Bouwens, R. J., Illingworth, G. D., Blakeslee, J. P., & Franx, M. 2006, *ApJ*, 653, 53
- Bouwens, R. J., et al. 2009a, *ApJ*, 705, 936
- . 2009b, *ApJ*, 690, 1764
- . 2011, *arXiv*, 1109.0994
- Bradley, L. D., et al. 2008, *ApJ*, 678, 647
- . 2011, *arXiv*, 1104.2035
- Broadhurst, T., et al. 2005, *ApJ*, 621, 53
- Calzetti, D., Armus, L., Bohlin, R. C., Kinney, A. L., Koornneef, J., & Storchi-Bergmann, T. 2000, *ApJ*, 533, 682
- Chabrier, G. 2003, *PASP*, 115, 763
- Coe, D., Benítez, N., Sánchez, S. F., Jee, M., Bouwens, R., & Ford, H. 2006, *AJ*, 132, 926
- Conroy, C., Gunn, J. E., & White, M. 2009, *ApJ*, 699, 486
- Ebeling, H., Edge, A. C., & Henry, J. P. 2001, *ApJ*, 553, 668
- Ebeling, H., Edge, A. C., Mantz, A., Barrett, E., Henry, J. P., Ma, C. J., & van Speybroeck, L. 2010, *MNRAS*, 407, 83
- Egami, E., et al. 2005, *ApJ*, 618, L5
- Finkelstein, S. L., et al. 2011, *arXiv*, 1110.3785
- Franx, M., Illingworth, G. D., Kelson, D. D., van Dokkum, P. G., & Tran, K.-V. 1997, *ApJ*, 486, L75
- Frye, B., Broadhurst, T., & Benítez, N. 2002, *ApJ*, 568, 558
- Gonzalez, V., Bouwens, R., Labbe, I., Illingworth, G., Oesch, P., Franx, M., & Magee, D. 2011, *arXiv*, 1110.6441
- Hall, N., et al. 2011, *arXiv*, 1101.4677
- Ilbert, O., et al. 2006, *A&A*, 457, 841
- Kneib, J.-P., Ellis, R. S., Santos, M. R., & Richard, J. 2004, *ApJ*, 607, 697
- Koekemoer, A. M., Fruchter, A. S., Hook, R. N., & Hack, W. 2002, in *The 2002 HST Calibration Workshop : Hubble after the Installation of the ACS and the NICMOS Cooling System*, ed. S. Arribas, A. Koekemoer, & B. Whitmore, 337
- Koekemoer, A. M., et al. 2011, *ApJS*, 197, 36
- Labbé, I., et al. 2010, *ApJ*, 716, L103
- Madau, P. 1995, *ApJ*, 441, 18
- Mann, A. W., & Ebeling, H. 2011, *arXiv*, 1111.2396
- Maughan, B. J., Jones, C., Forman, W., & Van Speybroeck, L. 2008, *ApJS*, 174, 117
- McLure, R. J., et al. 2011, *MNRAS*, 1787
- Merten, J., et al. 2011, *arXiv*, 1103.2772
- Moustakas, J., et al. 2011, *ApJ* submitted
- Oesch, P. A., et al. 2010, *ApJ*, 709, L21
- Postman, M., et al. 2011, *ApJS* submitted, *arXiv*, 1106.3328
- Richard, J., Kneib, J.-P., Ebeling, H., Stark, D. P., Egami, E., & Fiedler, A. K. 2011, *MNRAS*, 414, L31
- Schmidt, R. W., & Allen, S. W. 2007, *MNRAS*, 379, 209
- Stark, D. P., Ellis, R. S., Bunker, A., Bundy, K., Targett, T., Benson, A., & Lacy, M. 2009, *ApJ*, 697, 1493
- Vanzella, E., et al. 2011, *ApJ*, 730, L35
- Zheng, W., et al. 2009, *ApJ*, 697, 1907
- Zitrin, A., Broadhurst, T., Barkana, R., Rephaeli, Y., & Benítez, N. 2011a, *MNRAS*, 410, 1939
- Zitrin, A., Broadhurst, T., Coe, D., Liesenborgs, J., Benítez, N., Rephaeli, Y., Ford, H., & Umetsu, K. 2011b, *MNRAS*, 237
- Zitrin, A., et al. 2009, *MNRAS*, 396, 1985
- . 2011c, *arXiv*, 1103.5618